American Mineralogist, Volume 90, pages 22–27, 2005

Evidence for monazite-, barite-, and $AgMnO_4$ (distorted barite)-type structures of $CaSO_4$ at high pressure and temperature

WILSON A. CRICHTON,[1,*] JOHN B. PARISE,[2] SYTLE M. ANTAO,[2] AND ANDRZEJ GRZECHNIK[3]

[1]European Synchrotron Radiation Facility, B. P. 220, F-38043 Grenoble, France
[2]Dept Chemistry, Dept Geosciences and MPI, State University of New York, Stony Brook, New York 11794-2100, U.S.A.
[3]Laboratory of Crystallography, Universität Bayreuth, Bayreuth D-95440, Germany

ABSTRACT

Using laser-heated diamond-anvil cells, we have observed $CaSO_4$ undergoing phase transitions from its ambient anhydrite structure to the monazite type, and at highest pressure and temperature to crystallize in the barite-type structure. On cooling, the barite structure distorts from an orthorhombic to a monoclinic lattice to produce the $AgMnO_4$-type structure. The barite-structured form of $CaSO_4$ that we encounter at high pressure and temperature has been, in particular, long expected as a high-pressure phase of $CaSO_4$-anhydrite from systematic trends of similar $A^{II}B^{VI}O_4$-type sulfates, selenates, and tellurates, but has not been observed before. Similarly, the monoclinic distortion of the barite structure has itself been proposed as an intermediate phase between anhydrite and barite types through comparison with the phase diagrams of $NaBF_4$ and $NaClO_4$. This result has important consequences for identifying structural trends between different ABO_4-type phases of Group II sulfates, selenates, tellurates, chromates, molybdates and tungstates that crystallize in anhydrite, zircon, monazite, barite and scheelite-type structures at ambient and high pressures.

INTRODUCTION

Since the pioneering experimental work in the 1960s and 1970s that extended the phase diagrams of the $A^{2+}B^{6+}O_4$ sulfates, selenates, molybdates, and tungstates to pressures (*P*) up to 12 GPa and temperatures (*T*) up to ~1000 ºC, there has been considerable evidence for systematic trends in phase transitions in ABO_4 isotypes, based on relative cation size (Seifert 1968; Fukugana and Yamaoka 1979; Pannetier and Courtine 1966; Bastide 1987) and similarities with other cationic systems (Pistorius et al. 1969; Muller and Roy 1973; Liu and Bassett 1986). While these trends are now mostly well-established for binary oxides of $A^{(2+,3+,4+)}B^{(6+,5+,4+)}O_4$ stoichiometry, the situation with $CaBO_4$ (B = S, Se, Te) is intriguing. The stoichiometry $CaSO_4$ commonly crystallizes in hydrous and anhydrous forms as, respectively, gypsum and anhydrite. The structure adopted by anhydrite is not shared by any other of the $A^{2+}B^{6+}O_4$ chemistries; it does exist as both ammonium and potassium perchlorate (Gottfried and Schusterius 1932). Therefore its place, as an exception in the systematic, is of importance in establishing the trends of high *P* phase transitions between the "lower-*P*" (smaller cation) sulfates and chromates of $CrVO_4$- and zircon-types [e.g., $MgSO_4$, $MgCrO_4$, $CaCrO_4$ (chromatite); Rentzeperis and Soldatos 1958; Muller et al. 1969; Clouse 1932] and the anticipated "moderate-*P*" (larger cation) forms of sulfates and chromates that crystallize with monazite-and barite-type structures (e.g., $SrCrO_4$, $BaSO_4$, $RaSO_4$; Pistorius and Pistorius 1962; Jacobsen et al. 1998). If we extend this further, a link can then be constructed toward the "high-*P*" structures of the selenates, molybdates, and tungstates that form primarily primarily with barite- and scheelite-type structures (e.g., $SrSeO_4$, $BaSeO_4$, $RaSeO_4$, $SrMoO_4$, $BaMoO_4$, $RaMoO_4$, $CaMoO_4$, $CaWO_4$, $BaWO_4$, and $RaWO_4$; Pistorius and Pistorius 1962; Egorov-Tismenko et al. 1967; Guermen et al. 1971). It is therefore evident that understanding the high-*P* phase transformations of $CaSO_4$ in the broader framework of structural systematics is the key to successful anticipation of true high-*P* forms.

Given the relationships outlined above, it comes as little surprise that much effort has been made to identify post-anhydrite forms of $CaSO_4$, with the principle aim being to find the structural modification of $CaSO_4$ crystallizing with the barite structure. This has met with encouraging results (e.g., Borg and Smith 1975) in that the denser monazite ($CePO_4$)-form of $CaSO_4$ has been identified as the next high-*P* phase. This result confirmed that the larger-cation-hosting $SrSeO_4$ and $SrCrO_4$ (both monazites) are good model structures for the smaller cation $CaSO_4$ phase under high pressure. Nonetheless, observation of the barite variant, and its distorted $AgMnO_4$ precursor, which was also predicted by Pistorius et al. (1969) as a post-anhydrite phase, have remained elusive with the most recent study recovering an as yet unidentified ex situ orthorhombic structure from in situ high-*P* laser-heated Raman experiments (Chen et al. 2001). Although the barite phase was not found, Chen et al. (2001) did positively identify, through continuous observation of the *v*-SO_4 Raman bands, that the $[SO_4]^{2-}$ structural unit did remain intact over their entire *P-T* range, thus limiting the possible structures at high *P* (and *T*) to those with fourfold coordinated B cations. Nevertheless, there has been some doubt about the true sequence of the post-anhydrite phases of $CaSO_4$; scheelite ($CaWO_4$-type, adopted by $CaSeO_4$; e.g., JCPDS card 36-0932), $CaSeO_4$ [shown to also crystallize from the dihydrate in $P2_12_12_1$, Snyman and Pistorius (1963), though these authors consider the possibility that the structure is that of crocoite ($PbCrO_4$), i.e., monazite-

* E-mail: crichton@esrf.fr

0003-004X/05/0001–22$05.00/DOI:10.2138/am.2005.1654

type with $\beta \approx 90°$], barite ($BaSO_4$), $AgMnO_4$ (not previously encountered in Group II-VI oxides), and $AlTaO_4$ (adopted by $CaTeO_4$ and $SrTeO_4$; Hottentot and Loopstra 1979) all being reasonable candidates.

Here we report our findings on the high-*P* behavior of $CaSO_4$ using in situ X-ray powder diffraction data and combining laser-heating with diamond-anvil cells to achieve high *P*, *T* conditions simultaneously. Our results verify predictions of the high *P* structural systematics of ABO_4 compounds and we also demonstrate that structure selection rules are more sensitive to variation of pressure and temperature than is evident from empirical evidence based on the structures in the same Groups, identifying a richer sequence of phase transitions than those previously encountered in sulfates, selenates, and tellurates of Group II elements.

We have observed and positively identified three structure types of $CaSO_4$ at high *P*, *T*; the monazite type, the barite type, and its distorted-$AgMnO_4$ variant. In addition, we also have evidence for the existence of the orthorhombic structure first encountered by Chen et al. (2001). These structures can now be added to those known to exist at high temperature; those based on the mineral rhabdophane (trigonal-$CePO_4$; trigonal-$BiVO_4$ type) (Mooney 1950; Lager et al. 1984; Bezou et al. 1995) and rocksalt- or high-$NaClO_4$-like (Flörke 1952; Pistorius et al. 1969), to have a fuller understanding of the high *P*, *T* crystal chemistry of not only sulfates, but their Group VI and Cr-Group analogs, lanthanide phosphates and lanthanide silicates of ABO_4-type.' That is, delete comma and 'as well'.

Experimental methods

The starting material was a small piece of natural $CaSO_4$ from Bancroft, Ontario (Stony Brook collection no. 140019), ground to a fine powder in acetone and oven-dried. It was mixed with trace powdered pyrolytic graphite to obtain an even light-grey mixture that would heat under laser irradiation. The sample was loaded with a ruby sphere for pressure calibration (Mao et al. 1986) using the fluorescence method (Forman et al. 1972) in a stainless-steel gasket with a 125 µm diameter hole. In the loaded sample, the graphite was not detectable by diffraction. Two-dimensional diffraction data were collected with a MarResearch Mar345 image plate detector, previously calibrated and corrected for geometrical distortions using NBS SRM 660a (LaB_6 powder) with wavelength calibrated against the *I-K* edge, $\lambda = 0.3738(1)$ Å by the method outlined by Hammersley et al. (1995). At high *P* the sample was heated with an online YAG laser heating system. In the single-sided configuration used, the confocal laser and X-ray beams illuminated the sample during exposure and, simultaneously, thermal emission from the sample was collected with an Acton Research spectrometer and Jobin Yvon CCD via a reflecting objective for estimation of *T*. Additionally, during exposure the sample was moved in small increments so as to have an even coverage of the sample for increased averaging of powder statistics, whilst not overheating any region that might lead to crystallite growth and degradation of the powder pattern. The two-dimensional detector images were integrated to produce conventional one-dimensional 2θ-intensity patterns using Fit2D (Hammersley et al. 1996). The experiment was initially intended only as a reconnaissance to investigate the findings of Chen et al. (2001), thus data were only taken at a few points; at ambient conditions, at 11.5 GPa, at 21.4 GPa, and during heat treatment at nominally ~21 GPa and 1450 K. Once we observed crystallization of the new phase not described by Chen et al. (2001) we took steps to recover the sample, obtaining data on temperature quench and over several decompression steps.

Results

On increasing *P* to 11.8 GPa we obtained the monazite-type $CaSO_4$ phase first observed by Stephens (1964) and later by Borg and Smith (1975) as occurring at 2 GPa with a change in volume of about –4%. Rietveld refinement using the GSAS package of programs (Larson and von Dreele 1994) (Table 1; Fig. 1) returned cell parameters of $a = 6.3769(9)$, $b = 6.6439(9)$, and $c = 6.1667(8)$ Å, with $\beta = 102.220(10)°$ in space group $P2_1/n$ (cf. Borg and Smith 1975; with $a = 6.62$, $b = 6.91$, and $c = 6.35$ Å, and $\beta = 105.2°$ at ~3 GPa; JCPDS card 30-0279). With a unit-cell volume equal to $V = 255.35(6)$ Å^3, this is equivalent to a density of $\rho_{calc} = 3.541$ g/cm^3, or 19.7% higher than for anhydrite at ambient conditions ($\rho = 2.959$ g/cm^3). After further increasing *P* to 21.4 GPa, the laser was set at low power and focused on the sample, followed by a gradual increase in the power until thermal emission was visible. The sample was then scanned in the laser beam path so that a maximum volume was exposed to the laser. Diffraction patterns were then taken with simultaneous heating and collection of the thermal emission, from which we estimated the *T* to be 1450 K, with a variation in the Planck fit of < 30 K. The diffraction data collected under these conditions (nominally 21 GPa and 1450 K) was then used for cell indexing using CRYSFIRE (Shirley 2002). From a list of the first 20 peaks, based on their 2nd-derivatives, the highest figures of merit were obtained using both ITO (Visser 1969) and TAUP (Taupin 1973) [with $F(20) = 59.3$ and 49.9 respectively] for a primitive orthorhombic unit cell with $a = 6.3402$, $b = 7.5456$, and $c = 4.9542$ Å (ITO). While these cell parameters are not obviously close to those of the aristotype barite structure ($a = 7.1540$, $b = 8.8790$, $c = 5.4540$ Å in *Pbnm* for $BaSO_4$; JCPDS card 24-1035) a pattern calculated using POWDERCELL (Kraus and Nolze 1999) (with atomic positions for barite from Jacobsen et al. 1998 and our ITO cell parameters; substituting Ba for Ca and transforming the lattice setting to suit the space group symmetry) bore a sufficiently close resemblance to our pattern to warrant direct refinement with this initial model.

Using a 5-term background, refinement of peak-shape function (GU, GW, LX, assym), atomic positions, and anisotropic displacement parameters for each atom (45 parameters total), we obtained a fit with *R*p and *wR*p of 12.96% and 16.91%, respectively, and $\chi^2 = 2.748$ (Fig. 2; Table 2). The fitted cell parameters at nominal 21 GPa and 1450 K were $a = 6.3365(6)$, $b = 7.5347(7)$, and $c = 4.9532(5)$ Å for a unit-cell volume of $V = 236.52(4)$ Å^3 and $\rho_{calc} = 3.824$ g/cm^3. From comparison of this density with a hypothetical ambient density for the barite structure (e.g., Figure 3 of Chen et al. 2001; $\rho_{calc} = 3.151$ g/cm^3) we have a structure that is 21% more dense (at 1450 K and 21 GPa) than at ambient conditions and 29% more dense than anhydrite at ambient

Table 1. Results of Rietveld-refinement of monazite-type $CaSO_4$ at 11.8 GPa

Cell:	*a*		6.3769(9) Å	
	b		6.6439(9) Å	
	c		6.1667(8) Å	
	β		102.220(10)°	
	V		255.35(6) Å^3	
	space group	$P2_1/n$ (14)		
	ρ_{calc}		3.541 g/cm^3	
	*wR*p		11.54%	
	*R*p		8.96%	
	χ^2		1.853	
	x	*y*	*z*	U_{iso}
Ca	0.2685(8)	0.1592(9)	0.0981(10)	1.0
S	0.3036(11)	0.1664(14)	0.6278(11)	1.0
O1	0.2488(26)	0.0003(25)	0.4401(27)	2.5
O2	0.3573(34)	0.3480(22)	0.4915(25)	2.5
O3	0.4745(27)	0.1197(25)	0.7932(23)	2.5
O4	0.1192(27)	0.2202(22)	0.7110(23)	2.5

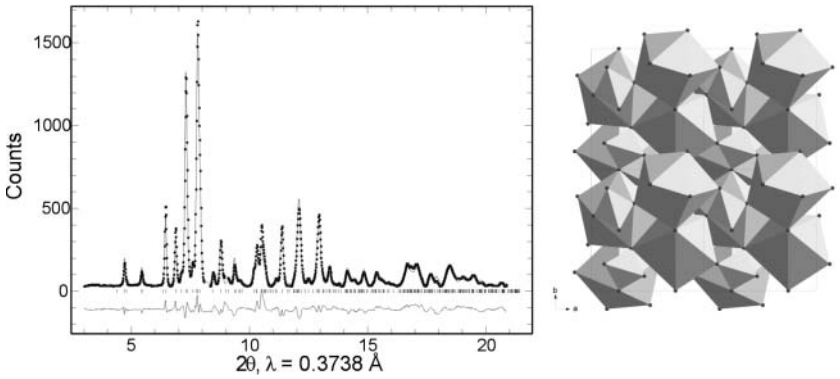

FIGURE 1. Final fit (solid line) to the observed powder diffraction data (dots) following Rietveld structure refinement (GSAS) of the monazite-type structure model for $CaSO_4$ (right) at 11.8 GPa and room temperature. The difference between the observed data and those calculated from the refined model is shown below on the same scale; vertical bars indicate positions of the allowed Bragg reflections.

conditions. Immediately on cooling we obtained evidence for a further phase transition through splitting of the (121) and (211) reflections and the appearance of numerous other peaks of lesser intensity throughout the pattern (Fig. 3). The general complexion of the pattern is similar to that of the barite phase at high *T*. Assuming this to be indicative of a structural similarity, we tried a subgroup of the barite structure as a first estimate of the true structure of $CaSO_4$ that gives rise to the pattern in Figure 3. Transforming *Pbnm*, through *Pnma* to $P2_1/n$ and adding a small distortion by setting $\beta = 91°$ resolved the splitting of the $(121)_{barite} \rightarrow (-121)_{mono} + (121)_{mono}$ and $(211)_{barite} \rightarrow (-112)_{mono} + (112)_{mono}$ peaks. A monoclinic distortion to a subgroup of the barite structure in $P2_1/n$ is sufficient to reproduce the experimental pattern, using an equivalent barite cell with a β angle $\neq 90°$. Given that this looked reasonably successful as a trial, we proceeded to test, firstly with indexing. KOHL (Kohlbeck and Hörl 1976) run from CRYSFIRE returned $a = 6.448$, $b = 7.595$, and $c = 5.085$ Å with $\beta = 91.664°$ and M(20) = 22.8 (at 11.8 GPa). The combination of unit cell and space group is very close to that predicted by Pistorius et al. (1969) for a possible intermediate phase between the anhydrite and barite structures, the $AgMnO_4$-type structure ($P2_1/n$, $a = 5.64$, $b = 8.33$, and $c = 7.12$ Å, $\beta = 92.25°$; JCPDS 20-0487; Boonstra 1967). From profile-fitting of the data obtained at 19.9 GPa (immediately on cooling from the barite phase at 1450 K, as shown in Fig. 3), we obtained cell parameters of $a = 4.9577(4)$, $b = 7.5243$ (4), and $c = 6.3397(7)$ Å, $\beta = 90.829(5)°$, and $V = 236.47(3)$ Å^3 (Table 3; Fig. 4) equivalent to a density of $\rho_{calc} = 3.824$ g/cm^3, very close to that of the barite-structured phase. It is unclear however, if the distortion leads to a 1st or 2nd-order transition.

Further reduction in *P* resulted in complete back-transformation to the anhydrite phase (Fig. 5). At this point, on opening and reclosing the DAC we noticed that there was an associated color change from gray (anhydrite + graphite, cell opened) to honey-color (DAC-closed). We re-exposed the decompressed sample with the cell closed finger-tight and observed new peaks that can be compared with those of Chen et al. (2001), who proposed an orthorhombic cell with $a = 6.602$, $b = 7.759$, and $c = 5.970$ Å from an assemblage of 70% anhydrite and 30% new orthorhombic phase. It is clear from comparing relative peak positions and intensities between our diffraction pattern and that of Chen et al. (2001) that we do not have the same ratio of anhydrite plus the proposed orthorhombic phase and that the cell parameters are slightly different (Fig. 5). Nonetheless, it does suggest that the phase is a low-*P* compound, obtained on recovery by Chen et al. (2001) and not that encountered by them at high *P*, *T*. We also point out that Chen et al. (2001) reported that the conditions for best preservation of the orthorhombic phase are *slow P* release from the high *P* state, contrary to what would normally be expected for recovery of a high-*P* phase in a metastable region.

TABLE 2. Results of Rietveld-refinement of barite-type $CaSO_4$ at 21 GPa and 1450 K

Cell:	*a*		6.3365(6) Å	
	b		7.5347(7) Å	
	c		4.9532(5) Å	
	V		236.52(4) Å^3	
	space group	*Pbnm* (62)		
	ρ_{calc}		3.824 g/cm^3	
	*wR*p		16.91%	
	*R*p		12.69%	
	χ^2		2.748	
	x	*y*	*z*	U_{iso}*
Ca	0.1696(6)	0.1812(6)	0.25	2.98(18)
S	0.8166(10)	0.5606(8)	0.25	4.52(21)
O1	0.5675(19)	0.8898(17)	0.25	3.34(21)
O2	0.5341(21)	0.2141(18)	0.25	3.34(21)
O3	0.3193(14)	0.4287(10)	0.9823(18)	3.34(21)

* $U_{iso} = Ui/Ue*100$; O1-O3 constrained to be equal.

TABLE 3. Results of profile-refinement of $AgMnO_4$-type $CaSO_4$ at 19.9 GPa

Cell:	*a*	4.9577(4) Å
	b	7.5243(4) Å
	c	6.3397(4) Å
	β	90.829(5) Å
	V	236.47(3) Å^3
	space group	$P2_1/n$ (14)
	ρ_{calc}	3.824 gcm^{-3}
	*wR*p	10.81%
	*R*p	7.75%
	χ^2	2.366

DISCUSSION

A commonly utilized rule of thumb in high-*P* synthesis and reconnaissance studies involves the use of compounds containing a larger cation, further down the same Group in the Periodic Table, as a proxy for reducing the pressure at which structural phase transitions occur. A good example of the implementation of this strategy is the low-*P* synthesis of germanates as analogues in studies of *P*-induced change in coordination from four- to sixfold in silicates. The substitution of Ge^{4+} for Si^{4+} increases the ionic

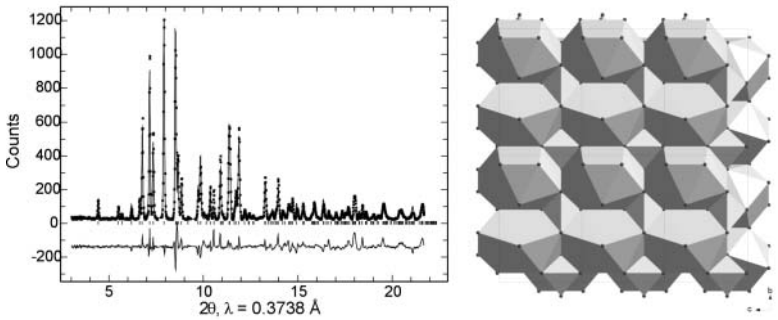

FIGURE 2. Final fit to the observed powder diffraction data following Rietveld structure refinement (GSAS) of the barite-type structure model for $CaSO_4$ (right) at nominal 21 GPa and 1450 K. Data points are as in Figure 1.

TABLE 4. Structures of $A^{2+}B^{6+}O_4$ (A = Mg, Ca, Sr, Ba, Ra; B = S, Se, Te, Cr, Mo, W) at ambient conditions

	SO_4	SeO_4	TeO_4
Mg	$CrVO_4$	barite	not described
Ca	anhydrite	$P2_12_12_1$*	$AlTaO_4$
Sr	barite	monazite	$AlTaO_4$
Ba	barite	barite	barite
Ra	barite	barite	not described
	CrO_4	MoO_4	WO_4
Mg	$CrVO_4$	$MnMoO_4$	wolframite
Ca	zircon	scheelite	scheelite
Sr	monazite	scheelite	scheelite
Ba	barite	scheelite	scheelite
Ra	barite	scheelite	scheelite

Note: $CaSeO_4$ formed from hydrate, $CaSeO_4$ also known to crystallize from solution in scheelite form

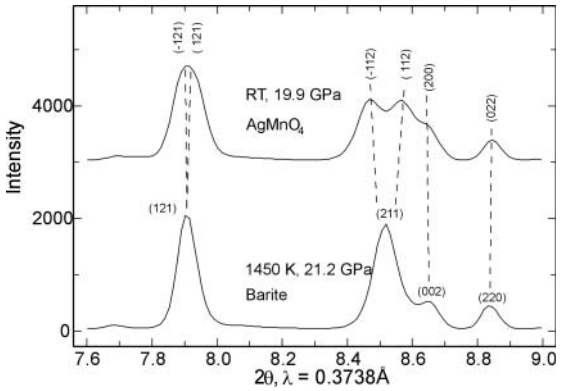

FIGURE 3. Diffraction patterns obtained on cooling from 1450 K to room *T*, showing the splitting of the barite (121) and (211) peaks, marking the distortion to the $AgMnO_4$ structure.

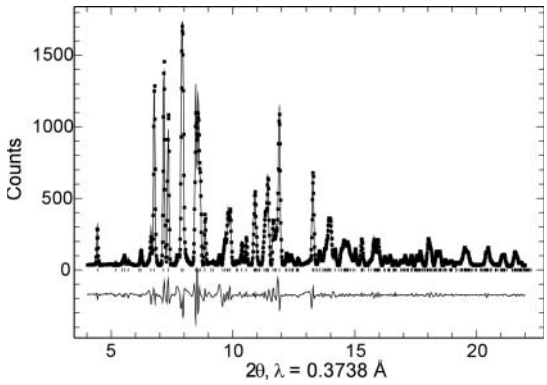

FIGURE 4. Profile-fitted diffraction pattern of the $AgMnO_4$-type structure of $CaSO_4$, also shown in Figure 6, at 19.9 GPa, on cooling from 1450 K. Data points as in Figure 1. Unfortunately, with the reduction in symmetry and increased number of parameters in the fit with respect to the data collected for the barite phase, it proved not prudent to proceed with full Rietveld analysis of the structure. This is probably due to excessive heating and recrystallization during collection of data for analysis of the barite-related phase, for which three individual heating treatments were made to ensure complete transformation.

radius of the substituted cation, mimicking the effect of *P*, which increases the cation:oxygen radii ratio and the coordination of the cation. In the case of $A^{2+}B^{6+}O_4$ compounds, Ca^{2+} in anhydrite ($CaSO_4$) is eightfold coordinated while Ba in barite ($BaSO_4$) is 12-coordinated. The $[SO_4]^{2-}$ group remains essentially unchanged in both structure types but the cation size at the A site increases from 1.12 Å (Ca^{2+} with coordination of 8) to 1.34 Å (Ba^{2+} with coordination of 12; Shannon 1976). In going down a Group, the cation:anion radius ratio will increase, favoring higher A cation coordination and mirroring the effects an increase in *P*.

Considering the structures of other Group II sulfates, particularly $BaSO_4$ and $BaSeO_4$, we should perhaps expect, in the broadest sense, the sequence of phases that we have observed (Table 4). While trends in high-*P* phase transformations can be predicted from associations like these (e.g., $CaSO_4$ will form barite, because $SrSO_4$, $BaSO_4$, and $RaSO_4$ all have the barite structure) they only give part of the story. Other aspects, such as the regularity and distortion of the polyhedra and of the overall structure, must be considered. For example, consider that the orthorhombic anhydrite-type is a distortion of the tetragonal zircon-type. In addition, the relative size of the cations (e.g., which cation is at the tetrahedral site proper; e.g., BPO_4 or PBO_4…), the cation valence and the ratio of A/B cation sizes together with the variation of A/B size with *P* affect the structure type at high *P*. It is probably this last point that makes if difficult to predict the structure observed at high *P* and partially explains why the sequences observed on compression, heating, and decompression are richer than anticipated based solely on considerations of radius ratio.

We have evidence for the $AgMnO_4$ permanganate phase, in addition to the Group II sulfate and selenate structures of anhydrite, monazite, and barite. Considering that the $AgMnO_4$ structure is indeed rare, it may not be expected that it form a series with anhydrite, based solely on the cation exchange within Groups. However, if we consider firstly, that we can obtain the $AgMnO_4$-type structure through a monoclinic disortion of the

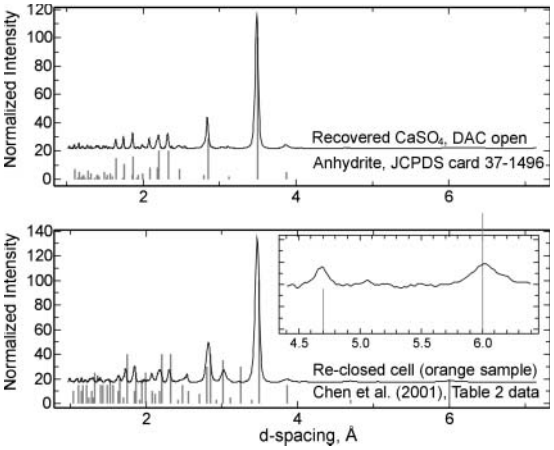

FIGURE 5. X-ray diffraction patterns of recovered anhydrite phase (top, continuous line) and on re-closing the DAC (bottom, continuous line) with grey vertical bars indicating peak positions of anhydrite and the data taken from Table 2 of Chen et al. (2001). In the insert the high *d*-spacing region of our sample and data from Chen et al. (2001) are displayed showing positions of (001) and (011) lines of their orthorhombic indexing. These peaks are distinct from anhydrite and from, for example, gypsum, $CaSO_4 \cdot 2H_2O$.

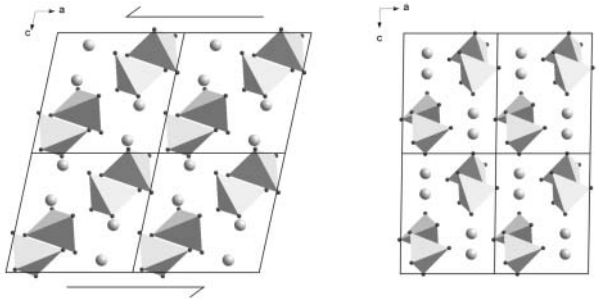

FIGURE 6. The monazite (left) and the $AgMnO_4$ (right) structures are closely related. It is evident from this diagram that a notional shear of the monazite structure parallel to **a**, reducing the β angle, would produce a topology close to that of $AgMnO_4$. Shown are SO_4-tetrahedra and cation positions, with non-bonded oxygen removed for clarity.

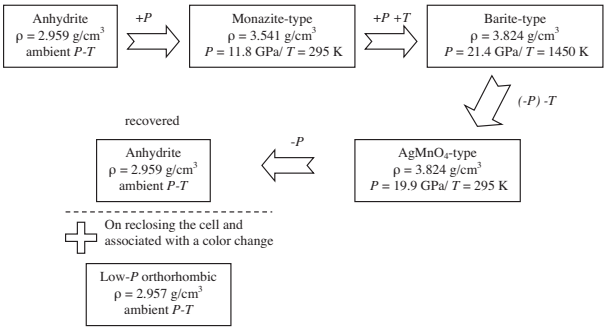

FIGURE 7. Schematic diagram of the phases encountered during our reconnaissance study, with *PT* positions (which do not imply equilibrium boundary positions) for each and their densities. Note that the initial recovered phase was solely anhydrite and that only on reclosing the cell a color change became apparent which was associated with the appearance of new peaks. The density information for proposed orthorhombic cell was obtained from Chen et al. (2001).

barite structure and secondly, that the topology of $AgMnO_4$ can be visualized through notional shearing of the monazite-type structure (Fig. 6), it is certainly reasonable that it should be a candidate as an intermediate between these two post-anhydrite phases. From the similarity of the phase diagram of $NaBF_4$ (ferruccite) with that of $NaClO_4$, Pistorius et al. (1969) identified the same four structural groups: high-*T* $NaClO_4$, anhydrite, barite, and $AgMnO_4$-type as an intermediate phase. Although the phase behavior at *P* of $CaSO_4$ was, at that time, little understood, we could assume a similar sequence (Fig. 7). In fact, barite, anhydrite, and monazite structures are already known for other ABF_4 chemistries at 1 bar (e.g., Köhler 1999; Köhler and Chang 1996). If we follow the reasoning of Borg and Smith (1975), we can see quite clearly why perchlorates, and $NaClO_4$ in particular, are good analogs of $CaSO_4$. In regularity and size of $[SO_4]^{2-}$ group, the closest resembling units are the $[PO_4]^{3-}$ and $[ClO_4]^{-}$ groups, with $[SeO_4]^{2-}$, $[CrO_4]^{2-}$, and $[SiO_4]^{4-}$ being similar. With respect to the size of the A cation in eightfold coordination, Ca^{2+} is most closely equivalent to Ce^{3+}, Bi^{3+}, Na^{1+}, Cd^{2+}, and Sr^{2+} (Shannon 1976). The natural connections to be made are therefore with the analogous $NaClO_4$, $CePO_4$, etc., which are encountered as their type structures (anhydrite and monazite, respectively) at 1 bar and also as their high *P*, *T* polymorphs (monazite, high-$NaClO_4$). Another example of the equivalence of these series is to be found in the lanthanide phosphates that crystallize with the monazite structure at 1 bar (those that crystallize as zircon will form monazite at high *P*). At high *T*, or through dimorphism, these can form the trigonal-$BiVO_4$ structure, as is known for the mineral rhabdophane, $CePO_4$ (Mooney 1950). At high *T*, through partial or complete dehydration of hemihydrates of $CaSO_4$, it has been observed that a trigonal hexagonal, or closely allied orthorhombic form has crystallized (Bushuev et al. 1983; Lager et al. 1984; Bezou et al. 1995) that is indeed rhabdophane-like.

Previous shock compression studies of $CaSO_4$ have indicated a phase transition between 36 and 54 GPa (Simakov et al. 1974) involving a change in density of 34% relative to ambient. Considering that our barite-structured phase has a density that is 29% greater (at 1450 K and 21 GPa), we can assume that it is likely that the greater part of the density difference obtained through shock compression is through our observed transition sequence, and that the additional 6% decrease in volume can probably be obtained through cooling of the barite phase and near-doubling of the *P*. However, this does not exclude the possibility of a further phase transition(s), which would most likely tend toward the scheelite-type structure (based on similar selenates, tellurates, tungstates, and fluorides at 1 bar, and zircons, monazites, molybdates, and chromates at high *P*; e.g. Wang et al. 2004). This common tetragonal structure is typified by the mineral $CaWO_4$ ($a = 5.242$ and $c = 11.37$ Å in $I4_1/a$, with density = 6.117 g/cm^3; JCPDS card 41-1431) and $CaSeO_4$ is also known in this form, JCPDS card 36-0293 (Snyman and Pistorius 1963). Perhaps the most intriguing question is, what would happen at still higher *P*-?

It has been demonstrated that $CaWO_4$ forms a fergusonite phase at high pressure in a situation similar to some lathanide tantalates and fluorides (Crichton and Grzechnik 2004; Grzechnik et al.

2003, 2002). Silicate zircons ($ZrSiO_4$, $HfSiO_4$) and, by inference, monazites, e.g., naturally dimorphous $ThSiO_4$ as thorite and huttonite (Taylor and Ewing 1978), have been observed to form firstly scheelite structures then, in some cases, to decompose to component oxides under high *P* conditions, Liu (1979, 1982). Similar behavior is also evident from work carried out on $ZrSiO_4$ at high *P-T* (Ono et al. 2004), at high-T from hydrothermally-prepared zircon and scheelite forms of $ZrGeO_4$ (Hirano and Morikawa 2003) and from fluoride scheelites; e.g. $LiGdF_4$, Grzechnik et al., 2004. We shall attempt futher studies on the sulfate systems to extend the sequence of ABO_4-phases into the post-barite p, T regime to link to the previously evidenced high-pressure behavior of silicates (such as zircon and silicate monazite) and molybdates and tungtates (scheelites and fergusonites).

ACKNOWLEDGMENTS

The diffraction data was collected at beamline ID30 of the European Synchrotron Radiation Facility during beamtime dedicated to in-house research. J.B.P. and S.M.A. are grateful for the support of NSF-EAR 0125094. We also thank G. Diego Gatta and S. Rath for their helpful reviews of the manuscript.

REFERENCES CITED

Bastide, J.P. (1987) Simplified systematics of the compounds ABX_4 ($X= O^{2-}, F^-$) and possible evolution of their crystal structures under pressure. Journal of Solid State Chemistry, 71, 115–120.

Bezou, C., Nonat, A., Mutin, J.-C., Nørlund Christensen, A., and Lehmann, M.S. (1995) Investigation of the crystal structure of γ-$CaSO_4$, $CaSO_4$·0.5H_2O, and $CaSO_4$·0.6H_2O by powder diffraction methods. Journal of Solid State Chemistry, 117, 165–176.

Boonstra, E.G. (1967) The crystal structure of silver permanganate. Acta Crystallographica, B24, 1053–1062.

Borg, I.Y. and Smith, D.K. (1975) A high pressure polymorph of $CaSO_4$. Contributions to Mineralogy and Petrology, 50, 127–133.

Bushuev, N.N., Maslennikov, B.M., and Borisov, V.M. (1983) Phase transformations in the dehydration of $CaSO_4$·2H_2O. Russian Journal of Inorganic Chemistry, 28, 1404–1407.

Chen, C., Liu, L., Lin, C., and Yang, Y. (2001) High-pressure phase transformation in $CaSO_4$. Journal of Physics and Chemistry of Solids, 62, 1293–1298.

Clouse, J.H. (1932) Investigations on the X-ray crystal structures of $CaCrO_4$, $CaCrO_4$·H_2O and $CaCrO_4$·$(H_2O)_2$. Zeitschrift für Kristallographie, Kristallgeometrie, Kristallphysik, Kristallchemie, 83, 161–171.

Crichton, W. A., and Grzechnik, A. (2004) Crystal structure of calcium molybdate, CaMoO4, a scheelite-type to fergusonite-type transition in powellite at P > 15 GPa. Zeitschrift fur Kristallographie NCS, in press, available at http://zkrist_ncs.cpfs.mpg.de/current.html

Egorov-Tismenko, Yu.K., Simonov, M.A., and Belov, N.V. (1967) Crystal structure of $SrMoO_4$. Kristallografiya, 12, 511–512.

Flörke, O.W. (1952) Die Hochtemperaturmodifikation von Kalzium-, Strontium- und Bariumsulfat. Naturwissenschafen, 39, 478–479.

Forman, R.A., Piermarini, G.J., Barnett, J.D., and Block, S. (1972) Pressure measurement made by utilisation of ruby sharp-line luminescence. Science, 176, 284–286.

Fukunaga, O. and Yamaoka, S. (1979) Phase transitions in ABO_4-type compounds under high-pressure. Physics and Chemistry of Minerals, 5, 167–177.

Gottfried, C. and Schusterius, C. (1932) Die Struktur von Kalium- und Ammoniumperchlorat. Zeitschrift für Kristallographie, Kristallgeometrie, Kristallphysik, Kristallchemie, 84, 65–73.

Grzechnik, A., Syassen, K., Loa, I., Hanfland, M., and Gesland, J.Y. (2002) Scheelite to fergusonite phase transition in $YLiF_4$ at high pressures. Physical Review B, 65, 104102.

Grzechnik, A., Crichton, W.A., Hanfland, M., and van Smallen, S. (2003) Scheelite $CaWO_4$ at high pressures. Journal of Physics: Condensed Matter, 15, 7261–7270.

Grzechnik, A., Crichton, W. A., Bouvier, P., Dmitriev, V., Weber, H.-P., and Gesland, J.-E. (2004) Decomposition of $LiGdF_4$ scheelite at high pressures. Journal of Physics: Condensed Matter, 16, 7779–7786

Guermen, E., Daniels, E., and King, J.S. (1971) Crystal structure refinement of $SrMoO_4$, $SrWO_4$, $CaMoO_4$, and $BaWO_4$ by neutron diffraction. Journal of Chemical Physics, 55, 1093–1097.

Hammersley, A.P., Svensson, S.O., Thompson, A., Graafsma, H., Kvick, Å., and Moy, J.P. (1995) Calibration and correction of distortions in two-dimensional detector systems. Review of Scientific Instruments, 66, 2729–2733.

Hammersley, A.P., Svensson, S.O., Hanfland, M., Fitch, A.N., and Haüsermann, D. (1996) Two-dimensional detector software: from real detector to idealised image or two-theta scan. High Pressure Research, 14, 235–248.

Hirano, M. and Morikawa, H. (2003) Hydrothermal synthesis and phase stability of new-zircon and scheelite-type $ZrGeO_4$. Chemistry of Materials, 15, 2561–2566.

Hottentot, D. and Loopstra, B.O. (1979) Structures of calcium tellurate, $CaTeO_4$, and strontium tellurate, $SrTeO_4$. Acta Crystallographica, B35, 728–729.

Jacobsen, S.D., Smyth, J.R., Swope, R.F., and Downs, R.T. (1998) Rigid-body character of the SO_4 groups in celestine, anglestite and barite. Canadian Mineralogist, 36, 1053–1060.

Kohlbeck, F. and Hörl, E.M. (1976) Indexing program for powder patterns especially suitable for triclinic, monoclinic and orthorhombic lattices. Journal of Applied Crystallography, 9, 28–33.

Köhler, J. (1999) Synthesis and structures of novel complex Yb(II) fluorides: YbBeF_4, $YbAlF_5$ and $LiYbAlF_6$. Solid State Sciences, 1, 545–553.

Köhler, J. and Chang, C.-H. (1996) Darstellung, Strukturen and Eigenshaften von $SmBeF_4$ und $SrBeF_4$–ungewoehnliche Varienten der Barytstruktur. Zeitschrift für Anorganische und Allgemeine Chemie, 622, 179–186.

Kraus, W., and Nolze, G. (1999) PowderCell for Windows V1.12. Federal Institute for Materials Research and Testing (BAM), Unter den Eichen 87, D-12205 Berlin. Program obtained via http://www.ccp14.ac.uk

Lager, G.A., Armbruster, T., Rotella, F.J., Jorgensen, J.D., and Hinks, D.G. (1984) A crystallographic study of the low-temperature dehydration products of gypsum, $CaSO_4$·2(H_2O); hemihydrate $CaSO_4$·0.50(H_2O) and γ-($CaSO_4$). American Mineralogist, 69, 910–918.

Larson, A.C. and Von Dreele, R. (1994) General Structure Analysis System (GSAS). Los Alamos National Laboratory Report LAUR, 86–748.

Liu, L. (1979) High-pressure phase transformations in baddeleyite and zircon, with geophysical implications. Earth and Planetary Science Letters, 44, 390 –396.

——— (1982) Phase transformations in the $MSiO_4$ compounds at high pressures and their geophysical implications. Earth and Planetary Science Letters, 57, 110–116.

Liu, L. and Bassett, W.A. (1986) High-pressure Phases with Implications for the Earth's Interior, pp. 146. Oxford University Press, New York.

Mao, H.K., Xu, J., and Bell, P.M. (1986) Calibration of the ruby pressure gauge to 800 kbar under-quasi-hydrostatic conditions. Journal of Geophysical Research, 91, 4673–4676.

Mooney, R.C.L. (1950) X-ray diffraction of cerous phosphate and related crystals I. Hexagonal modification. Acta Crystallographica, 3, 337–340.

Muller, O. and Roy, R. (1973) Phase transitions among the ABX_4 compounds. Zeitschrift für Kristallographie, 138, 237–253.

Muller, O., White, W.B., and Roy, R. (1969) X-ray diffraction of chromates of nickel, magnesium and cadmium. Zeitschrift für Kristallographie, 130, 112–120.

Ono, S., Tange, Y., Katayama, I., and Kikegawa, T. (2004) Equations of state of $ZrSiO_4$ phases in the upper mantle. American Mineralogist, 89, 185–188.

Pannetier, G. and Courtine, P. (1966). Sur un essai de systématique des composes du type ANO_4. Bulletin de la Société Chimique de France, 9, 2933–2938.

Pistorius, C.W.F. and Pistorius, M.C. (1962) Lattice constants and thermal-expansion properties of the chromates and selenates of lead, strontium and barium. Zeitschrift für Kristallographie, 117, 259–271.

Pistorius, C.W.F.T., Boeyens, J.C.A., and Clark, J.B. (1969) Phase diagram of $NaBaF_4$ and $NaClO_4$ to 40 kbar and the crystal-chemical relationship between the structures of $CaSO_4$, $AgMnO_4$, $BaSO_4$ and high-$NaClO_4$. High Temperature-High Pressure, 1, 41–52

Rentzeperis, P.J. and Soldatos, C.T. (1958) The crystal structure of the anhydrous magnesium sulphate. Acta Crystallographica, 11, 686–688.

Seifert, K.F. (1968) Untersuchungen zur Druck-Kristallchemie der AX_2-Verbindungen. Forschritte der Mineralogie, 45, 214–280.

Shannon, R.D. (1976) Revised effective ionic radii and systematic studies of interatomic distances in halides and chalcogenides. Acta Crystallographica, A32, 751–767.

Shirley, R. (2002) The Crysfire 2002 System for Automatic Powder Indexing: User's Manual, The Lattice Press, 41 Guildford Park Avenue, Guildford, Surrey GU2 7NL, England.

Simakov, G.V., Pavolvskiy, M.N., Kalsdhnikov, N.G., and Trunin, R.F. (1974) Shock compression of twelve minerals. Izvestiya Akademii Nauk SSSR Fizika Zemli 10, Earth Physics, 10, 488–492.

Snyman, H.C. and Pistorius, C.W.F.T. (1963) Some crystallographic properties of $CaSeO_4$ and its hydrates. Zeitschrift für Kristallographie, 119, 151–154.

Stephens, D.R. (1964) Hydrostatic compression of 8 rocks. Journal of Geophysical Research, 69, 2967.

Taupin, D. (1973) A Powder-Diagram Automatic-Indexing Routine. Journal of Applied Crystallography, 6, 380–385.

Taylor, M. and Ewing, R.C. (1978) The crystal structures of the $ThSiO_4$ polymorphs: Huttonite and thorite. Acta Crystallographica, B34, 1074–1079.

Visser, J.W. (1969) A fully automatic program for finding the unit cell from powder data. Journal of Applied Crystallography, 2, 89–95.

Wang, X., Loa, I., Syassen, K., Hanfland, M., and Ferrand, B. (2004) Structural properties of the zircon- and scheelite-type phases of YVO_4 at high pressure. Physical Review B, 70, 064109

MANUSCRIPT RECEIVED MARCH 23, 2004
MANUSCRIPT ACCEPTED JUNE 6, 2004
MANUSCRIPT HANDLED BY KARSTEN KNORR